



Global vegetation gross primary production estimation using satellite-derived light-use efficiency and canopy conductance



Marta Yebra^{a,c,d,*}, Albert I.J.M. Van Dijk^{a,c,d}, Ray Leuning^b, Juan Pablo Guerschman^d

^a Fenner School of Environment and Society, The Australian National University, ACT, Canberra, Australia

^b CSIRO Oceans and Atmosphere Flagship, ACT, Canberra, Australia

^c Bushfire & Natural Hazards Cooperative Research Centre, Melbourne, Australia

^d CSIRO Land and Water Flagship, ACT, Australia

ARTICLE INFO

Article history:

Received 12 December 2014

Received in revised form 19 March 2015

Accepted 20 March 2015

Available online 15 April 2015

Keywords:

Photosynthesis

Canopy conductance

Light use efficiency

FLUXNET

MODIS

Gross primary production

GPP

Vegetation

ABSTRACT

Climate and physiological controls of vegetation gross primary production (GPP) vary in space and time. In many ecosystems, GPP is primarily limited by absorbed photosynthetically-active radiation; in others by canopy conductance. These controls further vary in importance over daily to seasonal time scales. We propose a simple but effective conceptual model that estimates GPP as the lesser of a conductance-limited (F_c) and radiation-limited (F_r) assimilation rate. F_c is estimated from canopy conductance while F_r is estimated using a light use efficiency model. Both can be related to vegetation properties observed by optical remote sensing. The model has only two fitting parameters: maximum light use efficiency, and the minimum achieved ratio of internal to external CO_2 concentration. The two parameters were estimated using data from 16 eddy covariance flux towers for six major biomes including both energy- and water-limited ecosystems. Evaluation of model estimates with flux tower-derived GPP compared favourably to that of more complex models, for fluxes averaged; per day ($r^2 = 0.72$, root mean square error, RMSE = $2.48 \mu\text{mol C m}^2 \text{ s}^{-1}$, relative percentage error, RPE = -11%), over 8-day periods ($r^2 = 0.78$, RMSE = $2.09 \mu\text{mol C m}^2 \text{ s}^{-1}$, RPE = -10%), over months ($r^2 = 0.79$, RMSE = $1.93 \mu\text{mol C m}^2 \text{ s}^{-1}$, RPE = -9%) and over years ($r^2 = 0.54$, RMSE = $1.62 \mu\text{mol C m}^2 \text{ s}^{-1}$, RPE = -9%). Using the model we estimated global GPP of 107 Pg C y^{-1} for 2000–2011. This value is within the range reported by other GPP models and the spatial and inter-annual patterns compared favourably. The main advantages of the proposed model are its simplicity, avoiding the use of uncertain biome- or land-cover class mapping, and inclusion of explicit coupling between GPP and plant transpiration.

© 2015 Elsevier Inc. All rights reserved.

1. Introduction

The transport of CO_2 from the atmosphere into plant leaves, where it is used in photosynthesis, is inextricably linked to the simultaneous transport of water vapour in the opposite direction (transpiration). Plant physiological control of these opposing fluxes is exerted by stomata and the degree of control is quantified in terms of leaf stomatal conductance. At the ecosystem level, canopy conductances for water vapour (G_{cw}) and CO_2 (G_{cc}) provide links between transpiration and photosynthesis, respectively. Estimates of canopy conductance can be obtained by up-scaling stomatal conductances for all leaves in the canopy (Kelliher, Leuning, Raupach, & Schulze, 1995), or be inferred from ecosystem level measurements of exchanges of water vapour and CO_2 (Baldocchi, 2008). Both approaches have been shown to be suitable for application at canopy or local scales ($<1\text{--}2 \text{ km}$) but to derive regional or global estimates of canopy conductance, satellite remote sensing based methods are needed.

In a previous study, Yebra, Van Dijk, Leuning, Huete, and Guerschman (2013) used eddy covariance measurements of water vapour fluxes at 16 sites distributed globally to establish relationships between G_{cw} and Moderate Resolution Imaging Spectroradiometer (MODIS) reflectance observations. When the derived estimates of G_{cw} were combined with net radiation, wind speed and humidity deficit data, the resulting estimates of evapotranspiration (ET) were compared favourably with those from alternative approaches. Moreover, the method allowed a single parameterisation for all land cover types, which avoids artefacts resulting from errors in vegetation classification. In principle, the same satellite-derived G_{cw} values can be used within a process-based model for Gross Primary Production (GPP) while providing a direct link to the coupled energy and water balance of plant canopies.

In many ecosystems, GPP is limited by the amount of absorbed photosynthetically-active radiation (APAR), rather than by canopy conductance. The simplest approach to estimating GPP for these conditions is to multiply APAR by a light-use efficiency term (LUE or ϵ , mol C mol^{-1} APAR) representing the plant's capacity to convert light into fixed carbon (Running, Nemani, Glassy, & Thornton, 1999; Sims et al., 2008; Sjöström et al., 2011). This approach requires maximum LUE to be

* Corresponding author.

E-mail address: marta.yebra@anu.edu.au (M. Yebra).

modified where or when environmental conditions limit the rate of photosynthesis. In particular, a lack of soil water leads to stomatal closure, which reduces both ET and GPP. Over longer periods, sustained reduction in water availability will reduce vegetation cover, APAR and hence GPP (Andela, Liu, van Dijk, de Jeu, & McVicar, 2013).

In this paper the study of Yebra et al. (2013) is extended to allow the prediction of GPP globally. Our aim was to test a simple model that links GPP and ET through canopy conductance, while retaining the smallest number of ‘free’ fitting parameters necessary to construct a well-performing model that can be used at a global scale, without the need for ancillary information on land cover class. To account for the radiation limitation of GPP, we calibrate a simple LUE model that uses MODIS remote sensing data to estimate APAR, LUE and GPP. The lesser of the two estimates of GPP based on LUE or G_{cw} were assigned to each MODIS pixel encompassing a flux tower and globally. The results were then compared to the official MODIS GPP product (Zhao, Heinsch, Nemani, & Running, 2005) and to estimates from a regression tree approach (Jung, Reichstein, & Bondeau, 2009).

2. Theory

We use a ‘big-leaf’ description of the plant canopy and estimate the mean GPP (symbolised by F $\mu\text{mol C m}^{-2} \text{s}^{-1}$) as the lesser of conductance-limited and radiation-limited assimilation rates, denoted by F_c and F_r , respectively:

$$F = \min(F_c, F_r). \quad (1)$$

If it is assumed that transport of CO_2 from the bulk air to the intercellular leaf space is limited by molecular diffusion through the stomata, then F_c can be calculated from G_{cw} as:

$$F_c = c_g G_{cw} (1 - R_0) C_a \quad (2)$$

where G_{cw} (in m s^{-1}) is canopy conductance to water vapour and $R_0 = C_i/C_a$ the achieved *minimum* ratio of internal (C_i) to external (C_a) CO_2 concentration (mol mol^{-1}), and the conversion coefficient c_g (26 mol C m^{-3}) relates G_{cw} (m s^{-1}) to the conductance for CO_2 in molar units (G_{cc} , $\mu\text{mol C m}^{-2} \text{s}^{-1}$) (it can be calculated as $41.6 \text{ mol C m}^{-3}$ following the ideal gas law for standard air pressure and 25°C temperature, divided by 1.6 to account for the lesser diffusivity of CO_2 compared to H_2O). If it can be assumed that R_0 is constant for a given vegetation community or at least relatively narrowly constrained, then Eq. (2) can be used to estimate the maximum rate of CO_2 uptake for a given value of G_{cw} . Support for assuming a narrow range for R_0 is given by Figure 3c in Schulze, Kelliher, Korner, Lloyd, and Leuning (1994). They extracted data from the literature for maximum surface conductance (G_{sw}) and maximum assimilation rates (F_c) for various vegetation types across the globe. A plot of F_c versus G_{sw} (their Fig. 3C) yields a slope of 1.048 with an r^2 of 0.66. Using this value into Eq. (2) and $C_a = 360 \text{ ppm}$ results in $(1 - R_0) = 0.11$. The corresponding value of $R_0 = 0.89$ is for optimal conditions and is expected to be lower when various environmental factors limit photosynthesis (Tuzet, Perrier, & Leuning, 2003). Here we adopt a global value of $R_0 = 0.76$ which was obtained by fitting Eq. (2) to flux station data from 16 sites distributed globally across six biomes (see Section 4 below).

Radiation-limited GPP (F_r) was estimated using Eq. (3), where f_{PAR} is the fraction of absorbed PAR, Q is incident PAR ($\text{mol photons m}^{-2} \text{s}^{-1}$) and ε is a light use efficiency ($\text{mol C mol}^{-1} \text{ photons}$).

$$F_r = \varepsilon f_{PAR} Q \quad (3)$$

Most enzyme-mediated reactions have an optimum temperature range, and several other algorithms adjust GPP estimates for T (e.g. Yuan et al. (2007)). Consequently, temperature was tested for inclusion as part of algorithm development, but rejected because model

performance was only very marginally improved (see Supplementary material).

3. Data

3.1. MODIS-derived reflectances and canopy conductance to water vapour

The 16-day Terra-Aqua MODIS nadir reflectance product (MCD43A4, 500 m; Strahler, Muller, & Modis Sciences Team Members, 1999) provides surface reflectance corrected for the bidirectional reflectance distribution function (BRDF) and atmospheric effects, creating an apparent reflectance that is not affected by the location of the sensor relative to the pixel at the time of acquisition (Schaaf et al., 2002). Subsets of MCD43A4 data for each 500 m pixel containing a flux station were retrieved for the period 2000–2012 from the MODIS Web service (http://daac.ornl.gov/MODIS/MODIS-menu/modis_webservice.html) in order to calibrate and validate our approach. For global GPP estimates we used the 0.05° (ca. 5600 m) resolution MCD43C4 global reflectance product (collection 5) for the same period. The imagery was downloaded from the Land Processes Distributed Active Archive Center (LP DAAC, https://lpdaac.usgs.gov/data_access/data_pool) and the quality control and state flags were used to remove pixels with partial or complete cloud cover or low pixel quality in the study areas. Global estimates of canopy conductance based on remote sensing (G_{CRS}) were calculated as described by Yebra et al. (2013) for 8-day periods and at 0.05° spatial resolution. The calculations utilized three vegetation indices derived from the MCD43C4 reflectance product: the Enhanced Vegetation Index (EVI) (Huete et al., 2002), the Normalized Difference Vegetation Index (NDVI) (Rouse, Haas, Schell, Deering, & Harlan, 1974) and a crop coefficient (K_c) estimated following Guerschman et al. (2009). The data are available via <http://www.wenfo.org/wald/>.

3.2. Flux tower observations

The GPP estimates and meteorological data used in developing the model were derived from the ‘free fair-use’ Fluxnet LaThuile dataset (Agarwal et al., 2010). Following Yebra et al. (2013) we analysed 16 sites that have at least five years of data from 2000 onwards, to coincide with the period of MODIS data availability. The flux stations were surrounded by homogeneous land cover within 1 km from the measurement tower (Table 1) to ensure that the results are not compromised if some of the MODIS pixels are not fully centred on the tower (Goerner, Reichstein, & Rambal, 2009). Homogeneity was assessed visually, as judged by colour and texture, using high spatial resolution aerial and satellite images from various sources (Google Earth™ <http://earth.google.com>). The selected sites are located across several continents and included six major biomes, following the International Geosphere–Biosphere Programme classification scheme (Hansen, 2000): woody savannas (WSA), grasslands (GRA), croplands (CRO), evergreen needle-leaf (ENF), evergreen broadleaf (EBF) and deciduous broadleaf forest (DBF). In ecohydrological terms, both energy-limited (i.e., potential evaporation (PET) < precipitation (P)) and water-limited (PET > P) ecosystems are represented. Table 1 presents the values of a wetness index (WI), computed as the ratio between the long-term (1950–2000) annual average P and annual average PET. Sites with $WI > 1$ are described as energy-limited while areas with $WI < 1$ are termed water-limited. Here we define as

$$PET = \alpha_{PT} s R_n / (s + \gamma) \quad (4)$$

where s (Pa K^{-1}) is the slope of the saturation water vapour pressure versus temperature curve, γ is the psychrometric constant (Pa K^{-1}), R_n is absorbed net radiation (W m^{-2}) and $\alpha_{PT} = 1.26$ (Priestley & Taylor, 1972).

Half-hourly GPP and meteorological data were quality-checked using the flags included in the Fluxnet La Thuile dataset. Half-hourly

Table 1
Summary of the Fluxnet sites used in this study. WI, wetness index, computed as the ratio between the long-term (1950–2000) annual average precipitation and annual average potential evaporation. Climate refers to the Köppen and Geiger climate classification; Main Climates: (A) tropical rain climate, (C) warm temperate climate and (D) sub-arctic climate; Precipitation: (w) desert, (s) steppe, (f) fully humid and (s) summer dry; Temperature: (a) hot summer, (b) warm summer and (c) cool summer. IGBP stands for the International Geosphere–Biosphere Programme classification scheme. CRO: Crops; DBF: deciduous broadleaf forest; ENF and EBF: evergreen needle-leaf and broadleaf forest respectively; WSA: woody savannas; GRA: grasslands. MF: Mixed Forest; SAV: Savannas. MODIS-UMD presents the land cover type according to the Boston University's UMD classification scheme employed by MOD17.

Site code	Latitude (°)	Longitude (°)	Köppen	Precipitation (mm y ⁻¹) * = irrigated	Average temperature (°C)	WI	IGBP	MODIS-UMD	Vegetation description	Reference
AU–How	–12.49	131.15	Aw	1450	27	0.88	WSA	SAV	Seasonal tropical savannah	Beringer et al. (2003)
AU–Tum	–35.66	148.15	Cfb	1159	10.7	1.13	EBF	WSA	Wet temperate sclerophyll forest	Leuning, Cleugh, Zegelin, and Hughes (2005)
FI–Hyy	61.85	24.29	Dfc	620	2.2	1.07	ENF	ENF	Scots pine forest	Suni et al. (2003)
IT–Ro1	42.41	11.93	Csa	764	15.4	0.69	DBF	CRO	Young oak coppice	Rey et al. (2002)
IT–Ro2	42.39	11.92	Csa	760	15.4	0.69	DBF	WSA	Mature oak coppice	Tedeschi et al. (2006)
NL–Loo	52.17	5.74	Cfb	786	9.4	1.17	ENF	MF	Spruce plantation	Dolman, Moors, and Elbers (2002)
US–Bo1	40	–88.29	Dfa	991	11	0.91	CRO	CRO	Maize–soybean (rotation)	Meysers and Hollinger (2004)
US–Ha1	42.54	–72.17	Dfb	1071	6.6	1.14	DBF	DBF	Mixed deciduous forest	Urbanski et al. (2007)
US–Ho1	45.2	–68.74	Dfb	1070	5.3	1.21	ENF	MF	Mixed forest	Hollinger et al. (2004)
US–MMS	39.32	–86.41	Cfa	1031	10.9	0.97	DBF	DBF	Mixed deciduous forest	Schmid, Grimmond, Cropley, Offerle, and Su (2000)
US–Ne1	41.16	–96.48	Dfa	790*	10	0.72	CRO	CRO	Irrigated maize	Verma et al. (2005)
US–Ne2	41.16	–96.47	Dfa	789*	10	0.72	CRO	CRO	Irrigated maize–soybean rotation	Verma et al. (2005)
US–Ne3	41.18	–96.44	Dfa	784	10.1	0.72	CRO	CRO	Maize–soybean (rotation)	Verma et al. (2005)
US–Ton	38.43	–120.97	Csa	581	15.7	0.48	WSA	WSA	Oak savannah woodland	Ma, Baldocchi, Xu, and Hehn (2007)
US–Var	38.41	–120.95	Csa	544	15.9	0.44	GRA	WSA	Annual C3 grassland	Ma et al. (2007)
US–WCr	45.81	–90.08	Dfb	787	4	0.99	DBF	Mixed	Mixed forest	Cook et al. (2004)

values were averaged over daylight hours, defined as intervals with incoming shortwave radiation $> 5 \text{ W m}^{-2}$. The total daytime shortwave radiation (R_g , W m^{-2}) measured at the flux towers was used to calculate PAR assuming that the latter is 45% of the former (Howell, Meek, & Hatfield, 1983). This was converted to $\mu\text{mol photon m}^{-2} \text{ s}^{-1}$ by considering that 1 J of PAR corresponds to $\sim 4.4 \mu\text{mol photons}$.

3.3. Global meteorological data

Global estimates of daily GPP at 1° resolution were calculated using meteorological data produced using the methods as described in Sheffield, Goteti, and Wood (2006). These data are derived through a combination of reanalysis and field data and are available from Princeton University (<http://hydrology.princeton.edu>). The data used include 24 h mean downwelling shortwave radiation flux (R_g , W m^{-2}), specific humidity (q , $\text{m}^3 \text{ m}^{-3}$), air pressure (p , Pa) and minimum (T_{min} , K) and maximum (T_{max} , K) temperature for each day. To obtain daytime average R_g , the gridded data were divided by fraction daytime calculated using trigonometric equations. Daytime air temperature (T_a) was estimated using:

$$T_a = T_{min} + 0.75 (T_{max} - T_{min}). \quad (5)$$

Daytime vapour pressure deficit (D , Pa) was calculated as

$$D = e_{sat} - e \quad (6)$$

where e_{sat} (Pa) is saturation vapour pressure and e (Pa) the actual vapour pressure, estimated respectively as:

$$e_{sat} = 610.8 \times \exp\left(\frac{17.27 \times T_a}{T_a + 237.3}\right) \quad (7)$$

$$e = \frac{qp}{0.622} \quad (8)$$

where 0.622 is the ratio of the molar masses of water vapour and dry air.

4. Methods

For the first part of the analysis, the daily meteorological and flux data were used to derive G_{cw} by inverting the Penman–Monteith combination equation to yield:

$$G_{cw} = \frac{\lambda E G_a}{\frac{s}{\gamma} R_n - \left(\frac{s}{\gamma} + 1\right) \lambda E + \left(\frac{\rho c_p}{\gamma}\right) D G_a} \quad (9)$$

where λ is the latent heat of evaporation (MJ kg^{-1}), E is the evaporation rate ($\text{kg m}^{-2} \text{ s}^{-1}$), G_a is aerodynamic conductance (m s^{-1}), s the slope of the saturation vapour pressure versus temperature curve (Pa K^{-1}), γ the psychrometric constant (Pa K^{-1}), R_n net available energy (W m^{-2}), ρ air density (kg m^{-3}) and c_p the specific heat constant pressure of air ($\text{J kg}^{-1} \text{ K}^{-1}$).

We recognise that G_{cw} in Eq. (9) should strictly be surface conductance (G_{sw}) which accounts for both canopy transpiration (T) and evaporation from the soil (E_s). In this study we selected data corresponding to a dry canopy and soil surface (by only including observations after two days without precipitation) with $\text{NDVI} > 0.4$, conditions under which $E_s \ll T$ and hence $G_{cw} \approx G_{sw}$ (see Eq. (6) in Leuning, Zhang, Rajaud, Cleugh, and Tu (2008)).

Aerodynamic conductance G_a (m s^{-1}) was calculated using

$$G_a = \frac{1}{k^2 U} \ln\left(\frac{z-d}{z_0}\right) \ln\left(\frac{z-d}{z_{0H}}\right) \quad (10)$$

here k is the von Karman constant (0.40), U wind speed (m s^{-1}) at the measurement height (z) (m), d the zero-plane displacement (m) and z_0 and z_{0H} the roughness lengths for momentum and heat (m), respectively. The quantities d , z_0 and z_{0H} were estimated as $0.66h$, $0.123h$ and $0.0123h$, respectively, where h is canopy height (m).

The atmospheric concentration of CO_2 (C_a , mol mol^{-1}) was estimated for each day of the year (in fractional year, y) using a quadratic equation fitted to the CO_2 concentrations measured at Mauna Loa:

$$C_a = 1.206 \cdot 10^{-8} y^2 - 4.641 \cdot 10^{-5} y + 0.045. \quad (11)$$

The fraction absorbed PAR radiation (f_{PAR}) was calculated from the scaled Normalised Difference Vegetation Index ($NDVI^*$) derived from the MCD43A4 reflectance data, using the ramp function proposed by Donohue, Roderick, and McVicar (2008):

$$f_{PAR} = f_{PAR,max} NDVI^* \tag{12}$$

where $f_{PAR,max} = 0.95$ and

$$NDVI^* = \max \left(\min \left(\frac{NDVI - 0.1}{0.9 - 0.1}, 1 \right), 0 \right).$$

The assumptions underlying this function are that (a) surfaces with a $NDVI \leq 0.1$ have no vegetation cover, (b) surfaces with $NDVI \geq 0.90$ have full canopy cover, and (c) canopy cover increases linearly with $NDVI$ for intermediate values.

The remaining unknown variables in Eqs. (2) and (3) are R_0 and ε . The first of these was assumed to vary between sites but be invariant in time.

We used remotely sensed EVI to estimate ε (cf. Drolet et al., 2008; Goerner et al., 2009; Wu et al., 2009). EVI was developed to optimize the vegetation signal with improved sensitivity in high biomass regions and improved vegetation monitoring through de-coupling of the canopy background signal and a reduction in atmosphere influences (Huete et al., 2002). It was calculated from MCD43A4 reflectances, and similar to $NDVI$, EVI was scaled (denoted EVI^*) between values assumed to represent bare surfaces ($EVI = 0.05$) and vegetation with maximum feasible light use efficiency ($EVI = 0.9$) (A. Huete, University of Technology, Sydney, personal communication), before multiplying it with an estimated value of ε_{max} :

$$\varepsilon = \varepsilon_{max} EVI^* \tag{13}$$

where

$$EVI^* = \max \left(\min \left(\frac{EVI - 0.05}{0.90 - 0.05}, 1 \right), 0 \right).$$

During model development, we also tested alternative remote sensing predictors of ε , including $NDVI$, $GVMI$, unscaled EVI , $fPAR$ and G_{cRS} (cf. Yebra et al., 2013). Each was tested in isolation and in multiplicative

combinations of two indices. The formulation in Eq. (13) performed best for 12 out of 16 sites, as well as overall.

Initially, we used G_{cw} values directly derived from the flux tower data by inversion of the Penman–Monteith equation (Yebra et al., 2013) and optimized a single set of values of R_0 and ε_{max} across the 16 sites (cross-site optimization). Optimal values were found by minimizing the least squared difference between observed and modelled GPP, using the Levenberg–Marquardt nonlinear optimization algorithm adapted to Interactive Data Language (IDL, ITT Visual Information Solution, Inc.) by Markwardt (2008). The code (function MPFITFUN) is available from <http://purl.com/net/mpfit>. Subsequently, a similar optimization was performed, but this time for each site individually (per-site optimization), to assess the uncertainty in the model parameterization and the influence this had on model performance. In both cases this was assessed by comparing the difference between mean modelled and flux tower GPP in relative terms (relative predictive error, $RPE = (F_{Tower} - F_{Mod})/F_{Tower}$) and the Root Mean Square Error (RMSE).

Furthermore, the influence of temporal scale on model performance was assessed by calculating the same metrics at different time resolution (i.e., daily, weekly, monthly and annually).

4.1. Global GPP estimates

To test model performance at global scale, we first replaced the site-based G_{cw} estimates by values derived from the remote sensing product (G_{cRS}) of Yebra et al. (2013). Those estimates did not consider the possible effect of D on canopy conductance, although empirical evidence shows that stomatal conductance decreases with increasing D .

To determine if this effect needed to be accounted for, we tested whether the function proposed by Lohammar, Larsson, Linder, and Falk (1980) and Leuning (1995) could explain residual variance in the ratio of field-based over satellite-based conductance:

$$\frac{G_{cc}}{G_{cRS}} = \frac{C_0}{1 + D/D_{50}} \tag{14}$$

where C_0 is a coefficient to correct for the possibility that G_{cRS} may be an underestimate of its maximum value in saturated air (G_{cmax}), and D_{50} is the value of D at which canopy conductance is half of G_{cmax} .

Table 2

Quantitative measures of performance of the model for GPP at daily time scale. Predictions use canopy conductance derived from the flux tower and local meteorology. The parameters used are those derived from the cross-site optimization ($R_0 = 0.76$; $\varepsilon_{max} = 0.045 \text{ mol mol}^{-1}$) and per site (see R_0 and ε_{max} values for each site in this table). Allowable parameter ranges used in the optimization were 0.2–0.95 and 0.001–0.1 for R_0 and ε_{max} , respectively. RPE, relative predictive error; r^2 , coefficient of determination; RMSE, root mean square error ($\mu\text{mol C m}^2 \text{ s}^{-1}$). p_Fr (%) indicate the percentage of days that F is driven by radiation ($F_r < F_c$) for each site.

Site	Days	Cross-site optimization			Per-site optimization					p_Fr (%)
		RPE	r^2	RMSE ($\mu\text{mol C m}^2 \text{ s}^{-1}$)	R_0	ε_{max} (mol mol^{-1})	RPE	r^2	RMSE ($\mu\text{mol C m}^2 \text{ s}^{-1}$)	
AU–How	1307	7.43	0.74	1.31	0.81	0.043	–2.43	0.76	1.17	78
AU–Tum	1524	–32.49	0.52	2.65	0.72	0.064	–5.94	0.53	1.85	97
FI–Hyy	1232	–22.56	0.87	1.44	0.69	0.052	–8.68	0.87	1.20	85
IT–Ro1	1980	–2.36	0.80	1.37	0.68	0.034	–5.16	0.84	1.24	53
IT–Ro2	760	–10.36	0.79	2.19	0.71	0.053	6.00	0.79	2.05	55
NL–Loo	1488	–46.07	0.76	3.02	0.66	0.076	–11.93	0.77	1.76	90
US–Bo1	1402	–1.63	0.82	2.63	0.79	0.040	–13.43	0.82	2.52	88
US–Ha1	891	0.64	0.74	2.32	0.72	0.041	–4.26	0.75	2.29	73
US–Ho1	1055	–25.55	0.79	2.11	0.67	0.054	–6.14	0.79	1.68	58
US–MMS	945	45.83	0.80	3.75	0.79	0.025	–5.3	0.83	1.62	61
US–Ne1	788	–24.65	0.85	4.05	0.77	0.060	–5.36	0.85	3.27	95
US–Ne2	691	–12.05	0.85	3.34	0.77	0.051	–2.45	0.85	3.05	95
US–Ne3	732	–22.48	0.75	3.9	0.75	0.066	4.39	0.75	3.34	90
US–Ton	1805	–27.28	0.75	1.21	0.20	0.045	–11.79	0.75	1.03	52
US–Var	1195	8.60	0.89	1.29	0.82	0.040	–8.02	0.89	1.06	73
US–WCr	1090	20.28	0.81	3.15	0.71	0.035	–0.80	0.81	2.51	84
All	18,885	–10.99	0.72	2.48	–	–	–5.43	0.82	1.95	81
Min	691	–46.07	0.52	1.21	0.20	0.025	–13.43	0.53	1.03	52
Max	1980	45.83	0.89	4.05	0.82	0.076	6.00	0.89	3.34	97
Mean	1180	–9.04	0.78	2.48	0.70	0.049	–5.08	0.79	1.98	77

The proposed GPP model was subsequently applied at daily time steps and global scale for the period 2000–2011 with spatially uniform estimates for the two parameters using the 0.05° resolution MODIS canopy conductance product, and reflectance-derived NVDI and EVI values, combined with daytime PAR radiation, temperature and D calculated from the ‘Princeton’ meteorological dataset. These were done to examine which of the global datasets introduce the greatest uncertainty in monthly-mean GPP estimates.

For comparison, we downloaded two other global GPP datasets; the MODIS GPP product (MOD17A2, Zhao et al., 2005) and the Max-Planck Institute dataset (MPI, Jung et al., 2009) when data for both products were available for a common period (2000–2011). The MOD17A2 product is estimated with a conceptual process model that uses MODIS FPAR/LAI product (MOD15A2v5) and NCEP/NCAR reanalysis II meteorological data, with parameterisation based on a lookup table that was applied spatially using the MODIS land cover product (MOD12Q1v4) and modified based on performance against eddy-covariance GPP observations (Zhao et al., 2005). The MPI estimates were derived using a

regression tree model trained on eddy-covariance GPP estimates for 178 FLUXNET sites, with NDVI from the Advance Very High Resolution Radiometer (AVHRR) Global Inventory Modelling and Mapping Studies (GIMMS) product (until 2005) and SeaWiFS (2006–2011) sensors and ERA-interim reanalysis meteorological data as inputs (Jung et al., 2009). Therefore, although the approaches used to construct the three datasets differ, each uses a combination of optical vegetation density remote sensing and climate reanalysis and, to different degrees, are constrained by eddy-covariance observations.

5. Results

5.1. Parameter optimization

Table 2 lists values for R_0 and ϵ_{max} , optimized for each site. R_0 ranged between 0.66 and 0.82 for all sites except US-Ton with $R_0 = 0.20$, the lower limit of the parameter search space. Optimal values for ϵ_{max} ranged between 0.025 and 0.076 mol C mol⁻¹ photons. The average

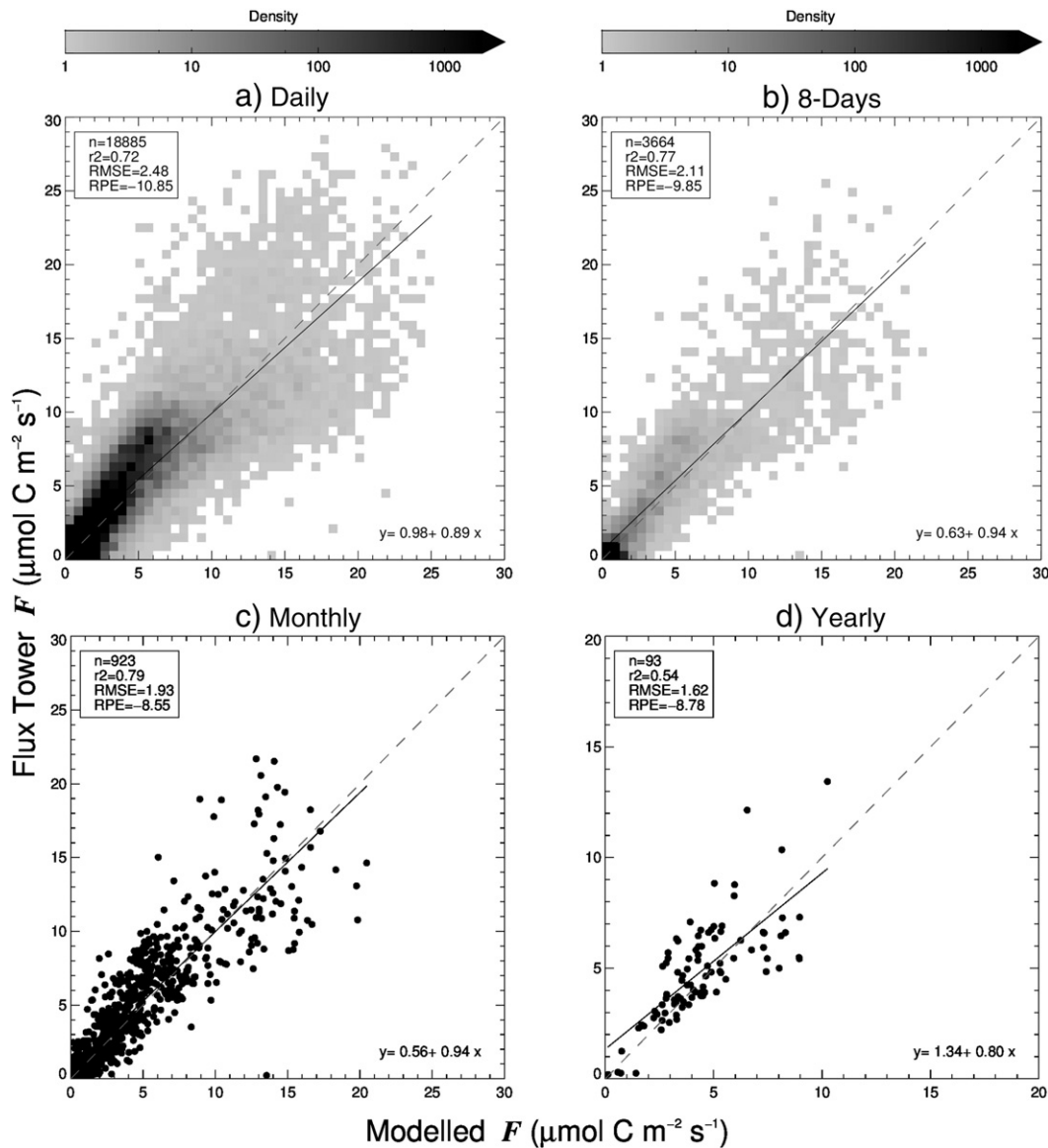


Fig. 1. Modelled GPP (F , $\mu\text{mol C m}^{-2} \text{s}^{-1}$) plotted against flux tower GPP at different time scales. Predictions use canopy conductance derived from the tower and local meteorology. The parameters used are those derived from the cross-site optimization ($R_0 = 0.76$ and $\epsilon_{max} = 0.045$). The short dash lines are 1:1 lines and the solid lines are linear regression lines. Also shown are statistics for model performance: n , number of cases; RMSE, root mean square error ($\mu\text{mol C m}^{-2} \text{s}^{-1}$); RPE, relative predictive error and r^2 , coefficient of determination.

value of R_0 was 0.7 (0.74 excluding the anomalous R_0 value obtained for US–Ton) and the mean ϵ_{max} was 0.049, values close to $R_0 = 0.76$ and $\epsilon_{max} = 0.045$, which are the overall optimized values for all sites combined.

5.2. Model evaluation against flux tower data

Model predictions of daily GPP using the uniform parameters ($R_0 = 0.76$, $\epsilon_{max} = 0.045 \text{ mol mol}^{-1}$), canopy conductance from the tower and local meteorology was strongly correlated with flux tower GPP ($r^2 = 0.72$, $\text{RMSE} = 2.48 \mu\text{mol C m}^2 \text{ s}^{-1}$ (Fig. 1a)). There was a negative bias in modelled GPP as shown by a RPE of -10.9% .

The model performed slightly better in reproducing 8-day and monthly average GPP values (Fig. 1b and c, respectively). This was evident from a higher r^2 (0.78 and 0.79), a lower RMSE (2.09 and $1.93 \mu\text{mol C m}^2 \text{ s}^{-1}$) and less negative bias (RPE of -9.8% and -8.6%) for 8-day and monthly values, respectively. Aggregation to annual

averages reduced the errors with respect to daily values ($\text{RMSE} = 1.62 \mu\text{mol C m}^2 \text{ s}^{-1}$, $\text{RPE} = -8.8\%$), (Fig. 1d), but r^2 decreased to 0.54.

Looking at the result of the cross-site optimization of R_0 and ϵ_{max} for individual sites, the RMSE ranged from 1.21 to $4.05 \mu\text{mol C m}^2 \text{ s}^{-1}$ and r^2 from 0.52 to 0.89 (Table 2). The per-site optimization described daily variations in GPP about equally well as the cross-site optimization (RMSE ranged from 1.03 to $3.34 \mu\text{mol C m}^2 \text{ s}^{-1}$ and r^2 from 0.53 to 0.89) (Table 2). However, the use of the values of R_0 and ϵ_{max} derived from the per-site optimization considerably decreased the RMSE and RPE at AU–Tum, NL–Loo and US–MMS, although the c values remained similar. Pooling data from the per-site optimization for all sites resulted in $r^2 = 0.82$, $\text{RMSE} = 1.95 \mu\text{mol C m}^2 \text{ s}^{-1}$ and $\text{RPE} = -5.43\%$.

Fig. 2 shows that the algorithm correctly predicted the timing of the annual cycle in GPP at each of the mid-latitude sites, largely because of the seasonal variation in incoming shortwave radiation, a key input to the model. In contrast, the seasonal amplitude of 8-day GPP is underestimated by 20–40% at five of the 16 sites (AU–Tum, NL–Loo,

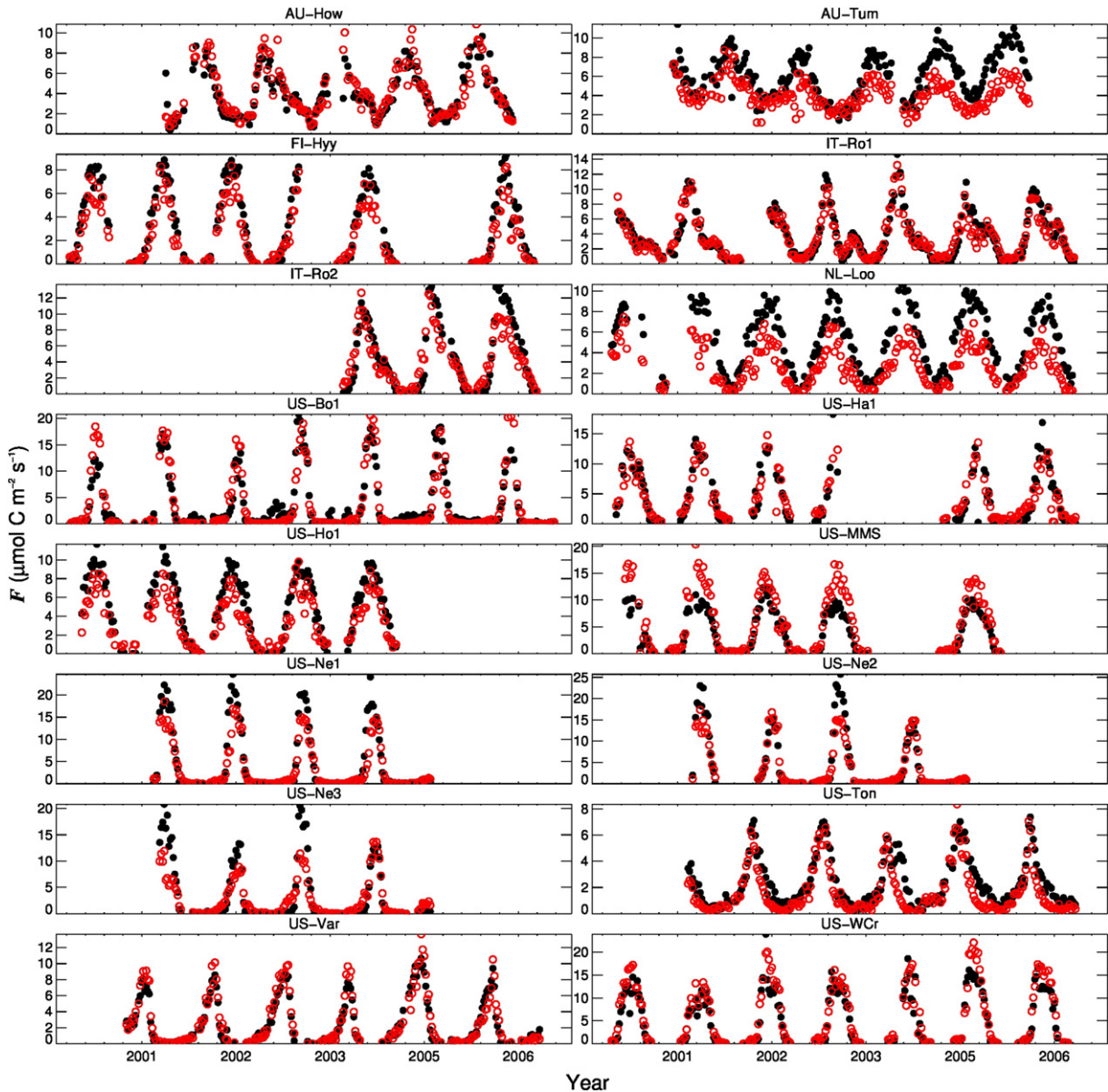


Fig. 2. Variation in predicted (red open circles) and flux tower (black filled circles) 8-day mean values of GPP (F , $\mu\text{mol C m}^2 \text{ s}^{-1}$) at model calibration sites. Predictions use canopy conductance derived from the tower and local meteorology. The parameters used are those derived from the cross-site optimization ($R_0 = 0.76$ and $\epsilon_{max} = 0.045 \text{ mol mol}^{-1}$).

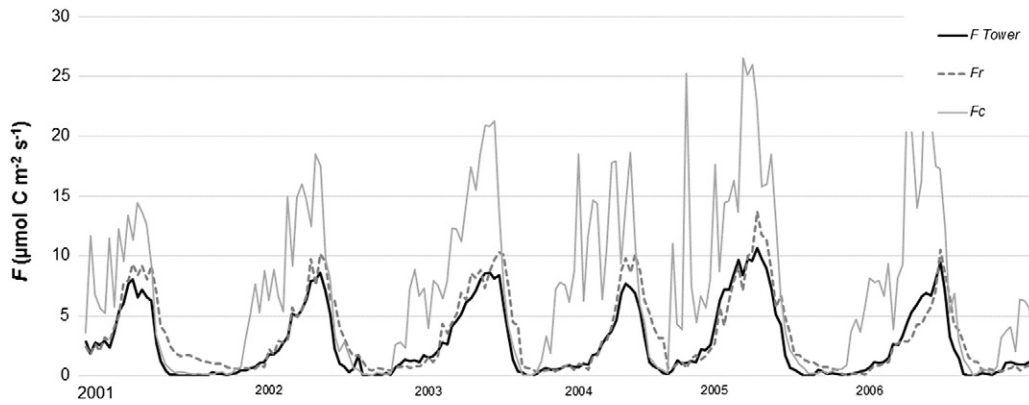


Fig. 3. Variation of 8-day mean values of GPP (F , $\mu\text{mol C m}^{-2} \text{s}^{-1}$) observed at US-Var and model estimates when GPP was conductance-limited (F_c) or radiation-limited (F_r). Predictions use canopy conductance derived from the tower and local meteorology. The parameters used are those derived from the cross-site optimization ($R_0 = 0.76$ and $\varepsilon_{max} = 0.045$). GPP was strongly limited by conductance during the hot dry summers but limited by radiation during the rest of the year.

US-Ne1, 2, 3) and is overestimated by a similar percentage at two others (US-MMS, US-WCr).

The model indicates that GPP is driven by radiation ($F_r < F_c$) for >50% of the time at each site ($52\% < p_{Fr} > 97\%$, Table 2). However, conductance plays an almost equally important role at IT-Ro1, IT-Ro2, US-Ton and US-Ho1 ($p_{Fr} \approx 50\%$) while solar radiation is the primary limiting factor at AU-Tum, NL-Loo, FI-Hyy, US-Bo1 and the Nebraska crop sites ($p_{Fr} \geq 85\%$).

Radiation and canopy conductance constrained GPP at different times during the growing season. For example, GPP at US-Var was strongly limited by conductance during the hot dry summers but was limited by radiation during the rest of the year (Fig. 3).

5.3. Response of satellite-derived canopy conductance to vapour pressure deficit

The ratios of canopy conductance derived from flux tower measurements to that based on satellite observations (G_{cw}/G_{CRS}) decreased by about 50% as D increased from 0.5 kPa to 2.5 kPa (Fig. 4). This result is consistent with the hyperbolic function used by Leuning (1995) for the response of stomatal conductance to D and confirms that the influence of

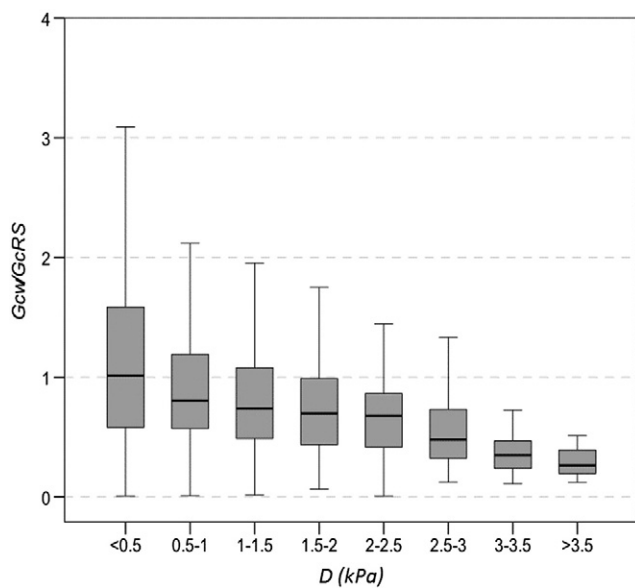


Fig. 4. Box plots showing the distribution of daily values of the ratio of flux tower derived canopy conductance (G_{cw} , derived from the PM approach) and modelled with remote sensing data (G_{CRS}) for different D intervals. Whiskers show the outer 5% percentiles.

D on canopy conductance can be accounted for by the same function. The values of C_0 and D_{50} in Eq. (14) were optimized across sites, producing values of $C_0 = 1.94$ and $D_{50} = 0.70$ kPa and these values were used to compute G_{CRS} .

5.4. Performance of global GPP estimates

Table 3 shows that replacing G_{cw} with G_{CRS} reduced r^2 by 7%, and increased the RMSE by 33%, while decreasing the magnitude of RPE. Replacing local with global meteorological data did not degrade the model performance appreciably. The greatest degradation in model performance was found when 0.05° reflectance data were used, although we consider model performance to be acceptable ($r^2 = 0.61$, RMSE = $2.65 \mu\text{mol C m}^{-2} \text{s}^{-1}$, RPE = -15%).

Despite its simplicity, the global version of our model (data available via <http://www.wenfo.org/wald/>) performed similar to MPI and MOD17 (Table 3). At monthly time scale, it produced the lowest RPE and performed better than MOD17 overall, although MPI achieved somewhat better r^2 and RMSE.

Application of the GPP algorithm with constant values for R_0 and ε_{max} gave an annual average global GPP of 107 Pg C y^{-1} for 2000–2011. Global estimates for the same period derived from MOD17 and MPI were $112 (+4\%)$ and $122 (+14\%) \text{ Pg C y}^{-1}$, respectively.

The global distribution of GPP shown in Fig. 5 is very similar to that in the MOD17 and MPI datasets (compared with Figure 1B in Beer et al., 2010). This agreement in distribution pattern is also seen in comparisons by latitude and by biome (Fig. 6). The latitudinal pattern in GPP

Table 3

Quantitative measures of model performance at monthly time scale when local data are replaced by estimates from global datasets. The parameters used are those derived from the cross-site optimization ($R_0 = 0.76$; $\varepsilon_{max} = 0.045 \text{ mol mol}^{-1}$ for the photosynthesis model and $D_{50} = 700$ and $C_1 = 1.94$ for the canopy conductance model). The performance of the MPI and MODIS algorithms for the same observations is included for comparison. RPE, relative predictive error; r^2 , coefficient of determination; RMSE, root mean square error.

Model	RPE (%)	r^2	RMSE ($\mu\text{mol C m}^{-2} \text{s}^{-1}$)
This study (site data)	-8.55	0.79	1.93
This study (with global G_{CRS})	-3.99	0.72	2.26
This study (with global meteorology)	-7.01	0.79	1.90
This study (with global G_{CRS} and meteorology)	-3.57	0.70	2.30
This study (with global G_{CRS} , meteo and reflectances)	-15.46	0.61	2.65
MPI	-17.95	0.73	2.36
MOD17	-27.57	0.50	3.15

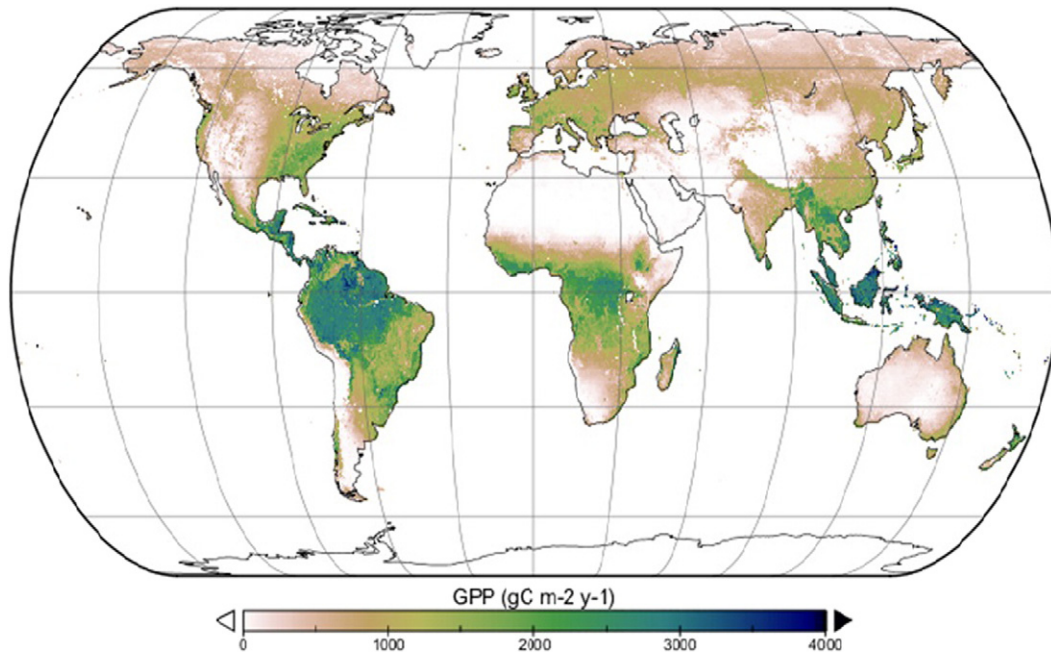


Fig. 5. Annual average gross primary production GPP ($\text{g C m}^{-2} \text{y}^{-1}$) estimates for the period 2000–2013.

is very similar for all three datasets but the magnitude of our estimates and of those from MOD17 are lower than those from MPI around 30°N and 15°S (Fig. 6a). Expressed per biome, our estimates were between those from the MOD17 and MPI for 4 out of 9 biomes (Fig. 6b). However, our GPP estimates are lower for water-limited and sparsely

vegetated ecosystems (low-latitude shrubland, savannas and ‘other’) and needleleaf forests.

Anomalies in annual global GPP relative to mean values for 2000–2011 are compared in Fig. 7 for the three datasets. Our algorithm yielded an inter-annual standard deviation ($\pm 0.65 \text{ Pg C y}^{-1}$) that is 30% lower than that from MOD17 (0.90 Pg C y^{-1}), but both were considerably less than that from the MPI dataset ($\pm 1.67 \text{ Pg C y}^{-1}$). There was some agreement in temporal anomaly patterns between our estimates and those from MOD17 ($r^2 = 0.34$, $\text{RMSE } 0.71 \text{ Pg C y}^{-1}$), but not with those from MPI ($r^2 = 0.17$, $\text{RMSE } 1.46 \text{ Pg C y}^{-1}$). Analysis per biome revealed that savannas and grasslands were the main source of inter-annual GPP variation in each of the datasets, and were responsible for most of the agreement with MOD17 ($r^2 = 0.81$) but also for much of the remaining disagreement ($\text{RMSE} = 0.35 \text{ Pg C y}^{-1}$). The sources of temporal disagreement between our estimates and those from MPI data were distributed across biomes.

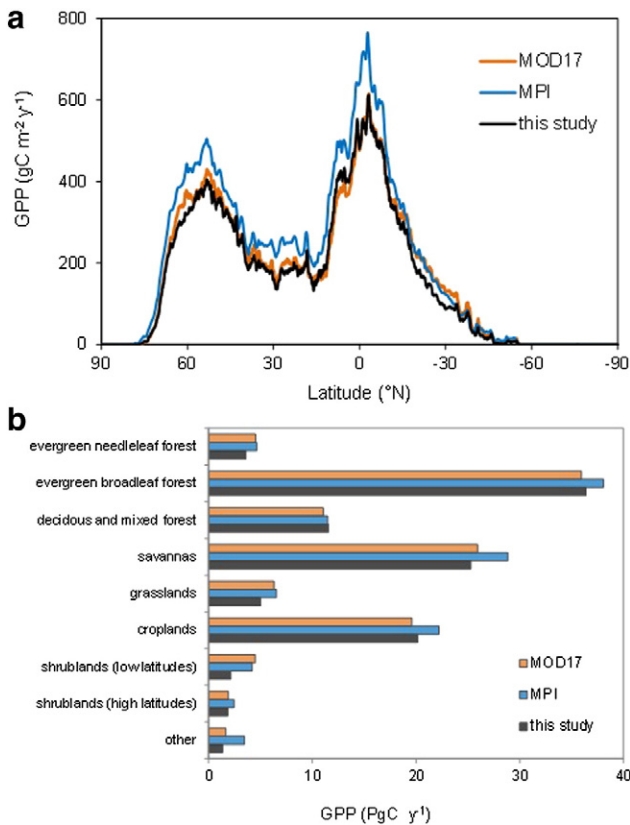


Fig. 6. Annual average terrestrial GPP for 2000–2011 calculated (a) for different latitudes (in $\text{g C m}^{-2} \text{y}^{-1}$; zero GPP was assigned to water bodies) (b) per generalised biome category (Pg C y^{-1}), using the MODIS land cover product (low latitudes are defined as within $\pm 60^\circ$).

6. Discussion

6.1. Site-to-site variation in model parameters

The average value for the two model-parameters R_0 and ϵ_{max} derived by model optimisation for each site was close to the overall optimized values for the 16 sites combined. However the analysis also showed site variability in the parameter values. NL-Loo obtained and optimized value of $\epsilon_{max} = 0.076$ and $R_0 = 0.66$ while for US-MMS values of $R_0 = 0.79$ and $\epsilon_{max} = 0.025$ were found. Therefore, the use of a single optimized intermediate value of ϵ_{max} and R_0 explains the overestimation of GPP for US-MMS and underestimation for NL-Loo.

Following Leuning (1995), our model predicts that there is a minimum achievable C_i/C_a ratio, R_0 , that determines maximum possible GPP for a given stomatal conductance. To test this, apparent C_i/C_a ratios can also be calculated directly from the observations, by rearranging Eq. (2) and inserting the measured GPP and G_{cw} that are derived from the flux tower measurements:

$$R_0 = 1 - \frac{F_w}{C_g G_{cw} C_a} \quad (15)$$

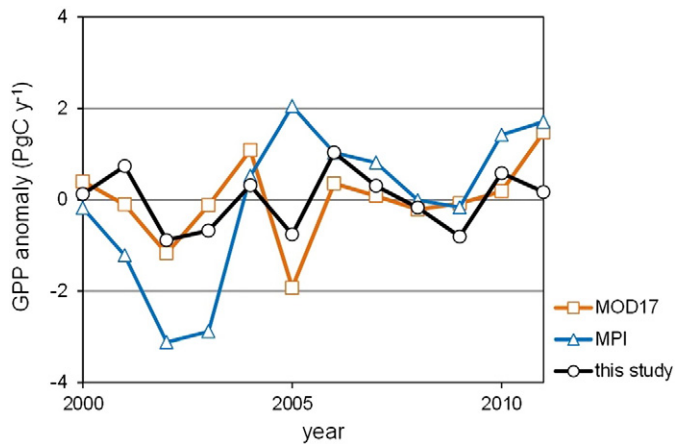


Fig. 7. Predicted annual global terrestrial GPP anomalies for 2000–2011 compared with values from the MODIS and MPI GPP datasets. Anomaly is defined as the difference between annual GPP and the GPP mean for 2000–11 (107 Pg C y^{-1}).

The main uncertainty in this approach is to determine on what days GPP was in fact limited by conductance, that is, when $F = F_w$, as required by Eq. (15). It can be assumed that VPD on such days was typically high.

The relationships found in Fig. 8 confirm the conceptual model, and agree with the general relationship between D and apparent C_i/C_a predicted by Leuning (1995). Values of C_i/C_a reach a minimum (R_0) around $D > 1.5 \text{ kPa}$, although not all sites experience high D values, making it difficult to determine R_0 for some of the sites. The relationship C_a varies between sites and suggests a dependence on vegetation type: needle-leaf forests and drought-adapted blue oaks (US–Ton) appear to have the lowest R_0 values, broadleaf forests have intermediate values, and crops and the (savannah) grasses (AU–How and US–Var) the highest values.

6.2. Model evaluation

There is good agreement between modelled and measured GPP at the 16 globally distributed flux stations at daily to yearly time scales. The highest errors were found for the Nebraska crop sites (US–Ne1, US–Ne2 and US–Ne3) and US–MMS although the r^2 values for these sites were still high (0.75–0.85). At US–Ne1 (maize), the peak in

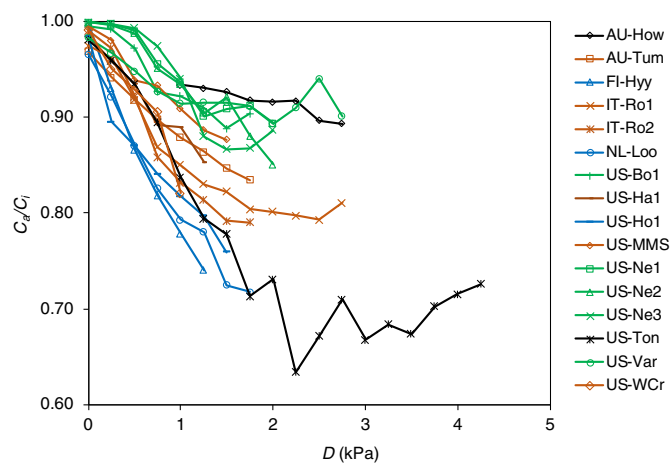


Fig. 8. Relationship between vapour pressure deficit (VPD, Pa) and the ratio of internal and external CO_2 concentrations (C_i/C_a) calculated from flux tower observations at 16 sites. Each point represents at least 10 days of data. Sites are coloured by IGBP vegetation type (blue = ENF, brown = DBF/EBF green = CRO/GRA, black = WSA; see caption Table 1 for meaning of codes).

GPP was always underestimated whereas for US–Ne2 and US–Ne3 (maize–soybean rotation sites) the peak was underestimated only for years with a maize crop (2001 and 2003) and not in seasons with a soybean crop. Maize assimilates CO_2 via a C4 fixation pathway. It is well-established that C4 species photosynthesise more effectively than C3 species and reach a maximum rate at lower radiation level. Consequently different ϵ_{max} values might be required for ecosystems dominated by C3 or C4 species. Still, Berry, Collatz, and DeFries (2003) developed an approach for capturing the spatial and temporal heterogeneity of both photosynthetic types by combining remote sensing products, physiological modelling, a spatial distribution of global crop fractions, and national harvest area data for major crop types. The derived information on the proportion of C3 and C4 plants per pixel used in such an approach could then be used in our algorithm (Donohue et al., 2014; Ryu et al., 2011). The main disadvantage is that this increases the complexity of the model and potentially degrades model performance due to considerable uncertainty in C3/C4 mapping.

Overall, our model captures the main factors that constrain photosynthesis. Radiation-limited photosynthesis dominated overall, but conductance played an almost equally limiting role at sites in Mediterranean climates with a lower wetness index ($WI < 0.69$). However, the influence of conductance limitation was also strong at US–Ho1 although this is a humid site ($WI = 1.21$). GPP was mainly driven by solar radiation at other temperate, continental and crop sites where water availability was usually adequate ($WI > 0.9$), confirming earlier studies (van Dijk, Dolman, & Schulze, 2005; van Gorsel et al., 2013).

Our model compares favourably against the accuracy of MPI and MOD17 as well as other published models. For example, the model of Yuan et al. (2010) explained about 75% and 61% of the variation of 8-day GPP estimates at calibration and validation sites, respectively, whereas our model explained 78% of 8-day tower GPP at calibration sites. Compared with the r^2 values reported by Yuan et al. (2010) (their Table 2) our model performed better at 6 sites (US–Bo, US–N1, 2, 3, US–WCr and US–Var, by 1–15%) and worse at two (US–Ton and US–Ho, by 5% and 9%, respectively). To compare our results with those of Ryu et al. (2011), we calculate the r^2 and RMSE modelled versus measured GPP for 7 sites common to both studies, for the year used in their analysis. Our model performed similarly at FI–Hyy, US–MMS and US–WCr, less well at US–Ne1 ($r^2 = 0.90$ and 0.75 , $\text{RMSE} = 2$ and $4 \text{ g C m}^{-2} \text{ d}^{-1}$ for Ryu et al. (2011) and this study, respectively) and better at AU–Tum (same r^2 but RMSE was $1.8 \text{ g C m}^{-2} \text{ d}^{-1}$ lower), AU–How ($r^2 = 0.30$ and 0.82 , $\text{RMSE} = 2.2$ and $0.9 \text{ g C m}^{-2} \text{ d}^{-1}$ for Ryu et al. (2011) and this study, respectively), and AU–Ton ($r^2 = 0.30$ and 0.71 , $\text{RMSE} = 1$ and $1.5 \text{ g C m}^{-2} \text{ d}^{-1}$ for Ryu et al. (2011) and this study, respectively).

6.3. Global estimates of GPP

Our analysis showed that using single, optimized parameter values ($R_0 = 0.76$; $\epsilon_{max} = 0.045 \text{ mol mol}^{-1}$) in our algorithm did not degrade model performance much compared to site-specific calibrations. This is perhaps surprising considering the site-to-site variability in locally optimized values, and may indicate that the model is more sensitive to model inputs than to the parameters. Additionally, using MODIS-derived canopy conductance (Yebra et al., 2013) did not strongly degrade model performance compared to using conductance derived from flux measurements. We extended the algorithm of Yebra et al. (2013) to account for the response of canopy conductance to D . The benefit of our conductance-based approach is that it produces mutually consistent estimates of GPP and transpiration, and therefore can be used to estimate canopy-level water use efficiency.

Further degradation was expected when global meteorological forcing data were used rather than site observations but the differences in model performance were small (Table 3). Overall the differences between gridded temperature and radiation estimates produced by Sheffield et al. (2006) and observations from the tower were modest

(results not shown). However, it is noted that most of the 16 sites are in regions with a relatively good measurement network. Errors are likely to be larger in some other parts of the world where measurement networks are less developed.

A second important advantage of the approach developed here is that identical coefficients can be applied globally to all land cover types. Although this increased RMSE slightly at some sites, when compared to using site specific parameters, it avoids errors induced by categorical land cover mapping. Table 1 shows that classification of half of the 16 sites differed between the Boston University's UMD classification scheme employed by MOD17, and the IGBP classification scheme. This misclassification affects the MODIS GPP estimates through the set of parameters that are applied to each pixel. Furthermore, our approach does not depend on indirect satellite-derived vegetation products such as LAI, which have been reported to increase errors in GPP estimation. For example, Ryu et al. (2011) found substantial overestimations of GPP at the AU–Tum site due to inaccuracies in MODIS LAI. They also found that underestimations of LAI during spring or autumn caused the underestimation of their model derived GPP in most needle-leaf forests.

Our global-average GPP estimates for 2000–2011 were 4% lower than those from MOD17 and 14% lower than those from MPI. Beer et al. (2010) estimated the range of plausible GPP estimates following the MPI machine learning method at $105\text{--}125\text{ Pg C y}^{-1}$; our estimate of 107 Pg C y^{-1} lies within that range. Furthermore, Ryu et al. (2011) estimated average GPP at $118 \pm 26\text{ Pg C yr}^{-1}$ for 2001–2003 and Yuan et al. (2010) reported a value of $111 \pm 21\text{ Pg C yr}^{-1}$ for 2000–2003; close to our values (also 107 Pg C y^{-1} for both periods).

When assessed by biome category, our GPP estimates were similar to MOD17 and MPI estimates for temperature and tropical humid biomes, but lower for needle-leaf forests and the most severely water-limited ecosystems.

The inter-annual pattern of global GPP predicted by our model is comparable to those in the MOD17 data, but both are considerably different from those in the MPI data. Zhao and Running (2010) showed that the MOD17 pattern agrees well with inter-annual variations in atmospheric CO_2 concentrations. In particular, the negative anomalies in both MOD17 and our own estimates (Fig. 7) could possibly explain, at least in part, accelerated CO_2 increases in the atmosphere in 2002 and 2005. On this basis, we conclude that the inter-annual GPP pattern derived from MPI, which has a strong positive anomaly in 2005, is less plausible. We speculate that data inconsistencies in the changeover from AVHRR GIMMS (up to 2005) to SeaWiFS (2006 onwards) may be a factor; annual anomalies appear to agree better during the latter period (Fig. 7).

7. Conclusions

The simple algorithm we propose for the estimation of GPP performs well at daily, monthly and annual time-scales and similarly well or better than other approaches published in the literature. The model was applied globally to compute global estimates of GPP using global meteorological data and MODIS nadir reflectances. The global spatial and temporal patterns in our GPP estimates compared favourably with other datasets. We consider this an encouraging result, given (a) the simplicity of our two-parameter model, (b) the lack of biome- or land-cover specific parameters, and (c) the simple but explicit coupling between ET and GPP. The site-based analysis and global comparison suggest that perhaps the greatest simplification made was the assumption that a minimum C_i/C_a ratio (i.e., R_0) of 0.75–0.85 is achievable in all ecosystems. We found some evidence that lower ratios are achieved by needle-leaf and drought-tolerant species, and higher ratios by crops and grasses (Table 2). Future research may help to find ways to better predict R_0 while still avoiding the use of uncertain categorical land cover maps.

Acknowledgments

This work used eddy covariance data acquired by the FLUXNET community and in particular by the following networks: AmeriFlux (U.S. Department of Energy, Biological and Environmental Research, Terrestrial Carbon Program (DE-FG02-04ER63917 and DE-FG02-04ER63911)), CarboEuropeIP, CarboItaly and OzFlux. We acknowledge the financial support to the eddy covariance data harmonization provided by CarboEuropeIP, FAO-GTOS-TCO, iLEAPS, Max Planck Institute for Biogeochemistry, National Science Foundation, University of Tuscia, Université Laval and Environment Canada and US Department of Energy and the database development and technical support from Berkeley Water Center, Lawrence Berkeley National Laboratory, Microsoft Research eScience, Oak Ridge National Laboratory, University of California-Berkeley, and University of Virginia. The support of the Commonwealth of Australia through the Cooperative Research Centre programme is acknowledged. We also acknowledge the contributions by Peter Hairsine, David Summers and four anonymous reviewers.

Appendix A. Supplementary data

Supplementary data to this article can be found online at <http://dx.doi.org/10.1016/j.rse.2015.03.016>.

References

- Agarwal, D. A., Humphrey, M., Beekwilder, N. F., Jackson, K. R., Goode, M. M., & van Ingen, C. (2010). A data-centered collaboration portal to support global carbon-flux analysis. *Concurrency and Computation: Practice and Experience*, 22, 2323–2334.
- Andela, N., Liu, Y. Y., van Dijk, A. I. J. M., de Jeu, R. A. M., & McVicar, T. R. (2013). Global changes in dryland vegetation dynamics (1988–2008) assessed by satellite remote sensing: Comparing a new passive microwave vegetation density record with reflective greenness data. *Biogeosciences*, 10, 6657–6676.
- Baldocchi, D. (2008). Breathing of the terrestrial biosphere: Lessons learned from a global network of carbon dioxide flux measurement systems. *Australian Journal of Botany*, 56, 1–26.
- Beer, C., Reichstein, M., Tomelleri, E., Ciais, P., Jung, M., Carvalhais, N., Rodenbeck, C., Arain, M., Baldocchi, D., Bonan, G., Bondeau, A., Cescatti, A., Lasslop, G., Lindroth, A., Lomas, M., Luysaert, S., Margolis, H., Oleson, K., Rouspard, O., Veenendaal, E., Viovy, N., Williams, C., Woodward, F., & Papale, D. (2010). Terrestrial gross carbon dioxide uptake: Global distribution and covariation with climate. *Science*, 329, 834–838.
- Beringer, J., Hutley, L. B., Tapper, N. J., Coutts, A., Kerley, A., & O'Grady, A. P. (2003). Fire impacts on surface heat, moisture and carbon fluxes from a tropical savanna in northern Australia. *International Journal of Wildland Fire*, 12, 333–340.
- Cook, B. D., Davis, K. J., Wang, W. G., Desai, A., Berger, B. W., Teclaw, R. M., Martin, J. G., Bolstad, P. V., Bakwin, P. S., Yi, C. X., & Heilman, W. (2004). Carbon exchange and venting anomalies in an upland deciduous forest in northern Wisconsin, USA. *Agricultural and Forest Meteorology*, 126, 271–295.
- Dolman, A. J., Moors, E. J., & Elbers, J. A. (2002). The carbon uptake of a mid latitude pine forest growing on sandy soil. *Agricultural and Forest Meteorology*, 111, 157–170.
- Donohue, R. J., Hume, I. H., Roderick, M. L., McVicar, T. R., Beringer, J., Hutley, L. B., Gallant, J. C., Austin, J. M., van Gorsel, E., Cleverly, J. R., Meyer, W. S., & Arndt, S. K. (2014). Evaluation of the remote-sensing-based DIFFUSE model for estimating photosynthesis of vegetation. *Remote Sensing of Environment*, 155, 349–365.
- Donohue, R. J., Roderick, M. L., & McVicar, T. R. (2008). Deriving consistent long-term vegetation information from AVHRR reflectance data using a cover-triangle-based framework. *Remote Sensing of Environment*, 112, 2938–2949.
- Drolet, G. G., Middleton, E. M., Huemmrich, K. F., Hall, F. G., Amiro, B. D., Barr, A. G., Black, T. A., McCaughey, J. H., & Margolis, H. A. (2008). Regional mapping of gross light-use efficiency using MODIS spectral indices. *Remote Sensing of Environment*, 112, 3064–3078.
- Goerner, A., Reichstein, M., & Rambal, S. (2009). Tracking seasonal drought effects on ecosystem light use efficiency with satellite-based PRI in a Mediterranean forest. *Remote Sensing of Environment*, 113, 1101–1111.
- Guerschman, J. P., Van Dijk, A. I. J. M., Mattersdorf, G., Beringer, J., Hutley, L. B., Leuning, R., Pipunic, R. C., & Sherman, B. S. (2009). Scaling of potential evapotranspiration with MODIS data reproduces flux observations and catchment water balance observations across Australia. *Journal of Hydrology*, 369, 107–119.
- Hansen, M. C. (2000). A comparison of the IGBP DISCover and University of Maryland 1 km global land cover products. *International Journal of Remote Sensing*, 21, 1365–1373.
- Hollinger, D. Y., Aber, J., Dail, B., Davidson, E. A., Goltz, S. M., Hughes, H., Leclerc, M. Y., Lee, J. T., Richardson, A. D., Rodrigues, C., Scott, N. A., Achuatavari, D., & Walsh, J. (2004). Spatial and temporal variability in forest-atmosphere CO_2 exchange. *Global Change Biology*, 10, 1689–1706.
- Howell, T. A., Meek, D. W., & Hatfield, J. L. (1983). Relationship of photosynthetically active radiation to shortwave radiation in the San-Joaquin Valley. *Agricultural Meteorology*, 28, 157–175.

- Huete, A., Didan, K., Miura, T., Rodriguez, E. P., Gao, X., & Ferreira, L. G. (2002). Overview of the radiometric and biophysical performance of the MODIS vegetation indices. *Remote Sensing of Environment*, 83, 195–213.
- Jung, M., Reichstein, M., & Bondeau, A. (2009). Towards global empirical upscaling of FLUXNET eddy covariance observations: Validation of a model tree ensemble approach using a biosphere model. *Biogeosciences*, 6, 2001–2013.
- Kelliher, F. M., Leuning, R., Raupach, M. R., & Schulze, E. D. (1995). Maximum conductances for evaporation from global vegetation types. *Agricultural and Forest Meteorology*, 73, 1–16.
- Leuning, R. (1995). A critical-appraisal of a combined stomatal-photosynthesis model for C-3 plants. *Plant, Cell and Environment*, 18, 339–355.
- Leuning, R., Cleugh, H. A., Zegelin, S. J., & Hughes, D. (2005). Carbon and water fluxes over a temperate Eucalyptus forest and a tropical wet/dry savanna in Australia: Measurements and comparison with MODIS remote sensing estimates. *Agricultural and Forest Meteorology*, 129, 151–173.
- Leuning, R., Zhang, Y. Q., Rajaud, A., Cleugh, H., & Tu, K. (2008). A simple surface conductance model to estimate regional evaporation using MODIS leaf area index and the Penman–Monteith equation. *Water Resources Research*, 44, W10419.
- Lohammar, T., Larsson, S., Linder, S., & Falk, S. O. (1980). FAST: Simulation models of gaseous exchange in Scots pine. *Ecological Bulletins*, 505–523.
- Ma, S., Baldocchi, D. D., Xu, L., & Hehn, T. (2007). Inter-annual variability in carbon dioxide exchange of an oak/grass savanna and open grassland in California. *Agricultural and Forest Meteorology*, 147, 157–171.
- Markwardt, C. B. (2008). *Non-linear least squares fitting in IDL with MPFIT*. Quebec, Canada: Astronomical Data Analysis Software and Systems XVIII.
- Meyers, T. P., & Hollinger, S. E. (2004). An assessment of storage terms in the surface energy balance of maize and soybean. *Agricultural and Forest Meteorology*, 125, 105–115.
- Priestley, C. H. B., & Taylor, R. J. (1972). On the assessment of surface heat flux and evaporation using large-scale parameters. *Monthly Weather Review*, 100, 81–92.
- Rey, A., Pegoraro, E., Tedeschi, V., De Parri, I., Jarvis, P. G., & Valentini, R. (2002). Annual variation in soil respiration and its components in a coppice oak forest in Central Italy. *Global Change Biology*, 8, 851–866.
- Rouse, J. W., Haas, R. W., Schell, J. A., Deering, D. H., & Harlan, J. C. (1974). *Monitoring the vernal advancement and retrogradation (Greenwave effect) of natural vegetation*. In *Greenbelt, MD, USA: NASA/GSFC*.
- Running, S., Nemani, R., Glassy, J., & Thornton, P. (1999). MODIS daily photosynthesis (PSN) and annual Net Primary Production (NPP) product (MOD17). *Algorithm theoretical basis document*. In *V. 3.0*.
- Ryu, Y., Baldocchi, D. D., Kobayashi, H., van Ingen, C., Li, J., Black, T. A., Beringer, J., van Gorsel, E., Knohl, A., Law, B. E., & Rouspard, O. (2011). Integration of MODIS land and atmosphere products with a coupled-process model to estimate gross primary productivity and evapotranspiration from 1 km to global scales. *Global Biogeochemical Cycles*, 25, GB4017.
- Schaaf, C. B., Gao, F., Strahler, A. H., Lucht, W., Li, X., Tsang, T., Strugnell, N. C., Zhang, X., Jin, Y., Muller, J. -P., Lewis, P., Barnsley, M., Hobson, P., Disney, M., Roberts, G., Dunderdale, M., Doll, C., d'Entremont, R. P., Hu, B., Liang, S., Privette, J. L., & Roy, D. (2002). First operational BRDF, albedo nadir reflectance products from MODIS. *Remote Sensing of Environment*, 83, 135–148.
- Schmid, H. P., Grimmer, C. S. B., Cropley, F., Offerle, B., & Su, H. -B. (2000). Measurements of CO₂ and energy fluxes over a mixed hardwood forest in the mid-western United States. *Agricultural and Forest Meteorology*, 103, 357–374.
- Schulze, E., Kelliher, F. M., Korner, C., Lloyd, J., & Leuning, R. (1994). Relationships among maximum stomatal conductance, ecosystem surface conductance, carbon assimilation rate, and plant nitrogen nutrition: A global ecology scaling exercise. *Annual Review of Ecology and Systematics*, 25, 629–662.
- Sheffield, J., Goteti, G., & Wood, E. F. (2006). Development of a 50-year high-resolution global dataset of meteorological forcings for land surface modeling. *Journal of Climate*, 19, 3088–3111.
- Sims, D. A., Rahman, A. F., Cordova, V. D., El-Masri, B. Z., Baldocchi, D. D., Bolstad, P. V., Flanagan, L. B., Goldstein, A. H., Hollinger, D. Y., Misson, L., Monson, R. K., Oechel, W. C., Schmid, H. P., Wofsy, S. C., & Xu, L. (2008). A new model of gross primary productivity for North American ecosystems based solely on the enhanced vegetation index and land surface temperature from MODIS. *Remote Sensing of Environment*, 112, 1633–1646.
- Sjöström, M., Ardö, J., Armeth, A., Boulain, N., Cappelaere, B., Eklundh, L., de Grandcourt, A., Kutsch, W. L., Merbold, L., Nouvellon, Y., Scholes, R. J., Schubert, P., Seaquist, J., & Veenendaal, E. M. (2011). Exploring the potential of MODIS EVI for modeling gross primary production across African ecosystems. *Remote Sensing of Environment*, 115, 1081–1089.
- Still, C. J., Berry, J. A., Collatz, G. J., & DeFries, R. S. (2003). Global distribution of C3 and C4 vegetation: Carbon cycle implications. *Global Biogeochemical Cycles*, 17, 1006.
- Strahler, A. H., Muller, J. P., & Modis Sciences Team Members (1999). *MODIS BRDF albedo product*. Algorithm theoretical basis document version 5.0, 53.
- Suni, T., Rinne, J., Reissell, A., Altimir, N., Keronen, P., Rannik, U., Dal Maso, M., Kulmala, M., & Vesala, T. (2003). Long-term measurements of surface fluxes above a Scots pine forest in Hyytiälä, southern Finland, 1996–2001. *Boreal Environment Research*, 8, 287–301.
- Tedeschi, V., Rey, A. N. A., Manca, G., Valentini, R., Jarvis, P. G., & Borghetti, M. (2006). Soil respiration in a Mediterranean oak forest at different developmental stages after coppicing. *Global Change Biology*, 12, 110–121.
- Tuzet, A., Perrier, A., & Leuning, R. (2003). A coupled model of stomatal conductance, photosynthesis and transpiration. *Plant, Cell & Environment*, 26, 1097–1116.
- Urbanski, S., Barford, C., Wofsy, S., Kucharik, C., Pyle, E., Budney, J., McKain, K., Fitzjarrald, D., Czirkowsky, M., & Munger, J. W. (2007). Factors controlling CO₂ exchange on time-scales from hourly to decadal at Harvard Forest. *Journal of Geophysical Research*, 112, G02020.
- van Dijk, A. I. J. M., Dolman, A. J., & Schulze, E. D. (2005). Radiation, temperature, and leaf area explain ecosystem carbon fluxes in boreal and temperate European forests. *Global Biogeochemical Cycles*, 19.
- van Gorsel, E., Berni, J. A. J., Briggs, P., Cabello-Leblic, A., Chasmer, L., Cleugh, H. A., Hacker, J., Hantson, S., Haverd, V., Hughes, D., Hopkins, C., Keith, H., Kljun, N., Leuning, R., Yebra, M., & Zegelin, S. (2013). Primary and secondary effects of climate variability on net ecosystem carbon exchange in an evergreen Eucalyptus forest. *Agricultural and Forest Meteorology*, 182, 248–256.
- Verma, S. B., Dobermann, A., Cassman, K. G., Walters, D. T., Knops, J. M., Arkebauer, T. J., Suyker, A. E., Burba, G. G., Amos, B., Yang, H. S., Ginting, D., Hubbard, K. G., Gitelson, A. A., & Walter-Shea, E. A. (2005). Annual carbon dioxide exchange in irrigated and rainfed maize-based agroecosystems. *Agricultural and Forest Meteorology*, 131, 77–96.
- Wu, C., Niu, Z., Tang, Q., Huang, W., Rivard, B., & Feng, J. (2009). Remote estimation of gross primary production in wheat using chlorophyll-related vegetation indices. *Agricultural and Forest Meteorology*, 149, 1015–1021.
- Yebra, M., Van Dijk, A., Leuning, R., Huete, A., & Guerschman, J. P. (2013). Evaluation of optical remote sensing to estimate actual evapotranspiration and canopy conductance. *Remote Sensing of Environment*, 129, 250–261.
- Yuan, W., Liu, S., Yu, G., Bonnefond, J. -M., Chen, J., Davis, K., Desai, A. R., Goldstein, A. H., Gianelle, D., Rossi, F., Suyker, A. E., & Verma, S. B. (2010). Global estimates of evapotranspiration and gross primary production based on MODIS and global meteorology data. *Remote Sensing of Environment*, 114, 1416–1431.
- Yuan, W. P., Liu, S., Zhou, G. S., Zhou, G. Y., Tieszen, L. L., Baldocchi, D., Bernhofer, C., Gholz, H., Goldstein, A. H., Goulden, M. L., Hollinger, D. Y., Hu, Y., Law, B. E., Stoy, P. C., Vesala, T., & Wofsy, S. C. (2007). Deriving a light use efficiency model from eddy covariance flux data for predicting daily gross primary production across biomes. *Agricultural and Forest Meteorology*, 143, 189–207.
- Zhao, M., Heinsch, F. A., Nemani, R. R., & Running, S. W. (2005). Improvements of the MODIS terrestrial gross and net primary production global data set. *Remote Sensing of Environment*, 95, 164–176.
- Zhao, M. S., & Running, S. W. (2010). Drought-induced reduction in global terrestrial net primary production from 2000 through 2009. *Science*, 329, 940–943.